Factors Influencing the Quality of Carbon Coatings on $LiFePO_4$

James D. Wilcox[a, c], Marca M. Doeff[a,*], Marek Marcinek[b], and Robert Kostecki[b]

a) Materials Sciences Division

b) Environmental Energy Technologies Division

Lawrence Berkeley National Laboratory

c) Department of Materials Science and Engineering

University of California

Berkeley, CA 94720

* mmdoeff@lbl.gov

Acknowledgment

This work was supported by the Assistant Secretary for Energy Efficiency and Renewable Energy, Office of FreedomCAR and Vehicle Technologies of the U.S. Department of Energy under contract no. DE-AC02-05CH11231.

Abstract

Several $LiFePO_4$/C composites were prepared and characterized electrochemically in lithium half-cells. Pressed pellet conductivities correlated well with the electrochemical performance in lithium half-cells. It was found that carbon structural factors such as sp^2/sp^3, D/G, and H/C ratios, as determined by Raman spectroscopy and elemental analysis, influenced the conductivity and rate behavior strongly. The structure of the residual carbon could be manipulated through the use of additives during $LiFePO_4$ synthesis. Increasing the pyromellitic acid (PA) content in the precursor mix prior to calcination resulted in a significant lowering of the D/G ratio and a concomitant rise in the sp^2/sp^3 ratio of the carbon. Addition of both iron nitrate and PA resulted in higher sp^2/sp^3 ratios without further lowering the D/G ratios, or increasing carbon contents. The best electrochemical results were obtained for $LiFePO_4$ processed with both ferrocene and PA. The improvement is attributed to better decomposition of the carbon sources, as evidenced by lower H/C ratios, a slight increase of the carbon content (still below 2 wt. %), and more homogeneous coverage. A discussion of the influence of carbon content vs. structural factors on the composite conductivities and, by inference, the electrochemical performance, is included.

Introduction

Significant attention has been directed towards developing $LiFePO_4$ as a possible cathode replacement for $LiCoO_2$ in lithium-ion batteries, after the initial report by Padhi *et al.* in 1997.[1] Low toxicity, the potential for low cost, and excellent stability during normal cycling and storage conditions make this material particularly attractive for large-scale applications such as hybrid electric vehicles (HEVs) and electric vehicles (EVs). Charge and discharge proceeds via a two-phase reaction[2] between $LiFePO_4$ and $FePO_4$, giving a flat discharge profile at ~3.45 V vs. Li/Li^+ and a reversible theoretical specific capacity of 170 mAh/g. $LiFePO_4$, however, suffers from low intrinsic rate capability, which has been ascribed to the slow diffusion of lithium ions across the two-phase boundary and low electronic conductivity, calculated to be about 10^{-9} S cm^{-1}.[3]

Numerous approaches directed at overcoming these problems have been described in the literature. These include the mixing in of fine metal particles,[4] systematic control of reaction parameters to control particle size and morphology,[5,6,7,8] and attempts at doping with supervalent cations in the lithium site to create a *p*-type semiconductor.[9] (Recent results[10] indicate, however, that true substitution does not occur; rather a nano-network of impurity phases including iron phosphides form, which enhances the pressed pellet conductivities considerably). One of the most promising avenues is the addition of conductive carbon either post-synthesis (e.g., by co-grinding),[11] or by co-firing with organic or polymeric additives to produce coated particles.[12,13,14,15] To avoid decreasing the energy density unduly, the amount of carbon should be kept low.[16] An interesting observation is that electrode performance does not always track with the amount of carbon in $LiFePO_4$/C composites.[17] The structure of the carbon, particularly the sp^2/sp^3 and D/G

(disordered/graphene) ratios, strongly influences the electronic conductivity. Samples containing smaller amounts of high-quality carbon (i.e., those having high sp^2/sp^3 and low D/G ratios) can outperform those containing larger amounts of a less-conductive coating. It has also been shown that the structure of the carbon in these composites produced by co-firing depends upon the source (i.e., type of organic or polymeric precursor), as well as the processing conditions.[18] Optimization of the carbon structure should allow the amount required to overcome the conductivity limitations of $LiFePO_4$ to be minimized. This paper describes our recent experimental work directed towards this goal.

The low temperatures (typically ~600-750°C) used in the preparation of $LiFePO_4$ present a challenge for the co-production of well-ordered, graphitic carbon *in-situ*. [18] Nevertheless, it is possible to manipulate the synthesis conditions to produce carbons with more desirable characteristics. In particular, the judicious selection of carbon sources and graphitization catalysts can result in markedly improved coatings, as will be shown below.

Experimental

$LiFePO_4$ samples were made via a sol-gel synthesis using $Fe(NO_3)_3 \cdot 9H_2O$ (iron nitrate, Sigma Aldrich 98+%), $C_2H_3O_2Li \cdot 2H_2O$ (lithium acetate, Sigma Aldrich), and H_3PO_4 (phosphoric acid, EMP, 85%). The iron nitrate and lithium acetate were combined with the phosphoric acid in a stoichiometric ratio of 1:1:1. Distilled water was then added until all the constituents were completely dissolved. The solution was then slowly combined with two stoichiometric equivalents of $HOCH_2CO_2H$ (glycolic acid, Sigma Aldrich, 70% solution in water) and the pH was adjusted to between 8.5 and 9.5 using NH_4OH (ammonium hydroxide, EMD) to form the sol. The sol was then heated on a hot plate while stirring to evaporate the water from the solution and form the gel. Samples

were then fired to 500° C at a heating rate of approximately 3° C/min and held at temperature for 10 hours in a quartz tube furnace under flowing nitrogen to calcine the sample. Up to 8 wt. % pyromellitic acid ($C_6H_2(CO_2H)_4$, Sigma Aldrich, abbreviated PA from this point forward) and, optionally, iron nitrate, ferrocene ($C_{10}H_{10}Fe$, Alfa Aesar, recrystallized), or ferrocenecarboxylic acid ($C_{11}H_{10}O_2Fe$, Aldrich, 97%, abbreviated FCA from this point forward), ranging from 0.001-1 wt% were added to the samples, and mixtures were ground using a planetary ball mill in an appropriate solvent (ethanol or acetone) for one hour. The grinding solvent was then evaporated under a flow of nitrogen and the resulting powder was thoroughly mixed and fired to 600° C for ten hours.

Phase purity was determined by X-ray diffraction (XRD) on the resulting powders using a Philips X'Pert diffractometer using an X'Celerator detector with Cu Kα radiation (λ = 1.54 Å). Particle size distributions were resolved by means of a Beckman Coulter particle size analyzer (model LS 230) using Darvan*C (ammonium polymethacrylate, aqueous solution, R.T. Vanderbilt Company Inc.) as a dispersant. Particle morphology studies were conducted using a field emission-scanning electron microscope (FE-SEM, Jeol JSM-6340F). Luvak Inc. (Boylston, MA) conducted the elemental analyses (carbon and hydrogen) of several samples.

An integrated confocal Raman microscope system, "Labram," made by ISA Group Horiba was used to analyze the structure of the active materials. Raman spectroscopy measurements were carried out at room temperature in ambient atmosphere using an internal He-Ne 632 nm laser was used as the excitation source. The power of the laser beam was adjusted to 0.1 mW with neutral filters of various optical densities. The size of the laser beam at the sample was ~1.2 μm, and the average acquisition time for each spectrum was

25 seconds. The resolution of this instrument is approximately 1.7 cm^{-1}. Baseline correction and deconvolution analysis of Raman spectra were performed with a commercial software package (PeakFit, version 4.05, SPSS Inc.).

Pressed pellets for conductivity studies were fabricated by uni-axially pressing ~0.5 g of active material to 10 kpsi in a ½" stainless steel die. The pellets were then transferred into balloon holders and cold isostatically pressed to 180 kpsi achieving a final density of ~70% of the theoretical $LiFePO_4$ density (3.6 g/cm^3). Thin gold electrodes were then sputtered on to each face of the pellet using a Bal-Tec SCD 050 sputter coater. AC impedance spectra were obtained using a Solartron Instruments 1260 impedance/gain-phase analyzer at selected temperatures between 25 and 200° C. Conductivities were derived from the touchdown of the capacitative arc in the Nyquist plots.

Electrodes were composed of 80 wt% active material, 8 wt% Kynar poly(vinylidene fluoride) (PVDF) (Elf Atochem North America Inc., Technical Polymers Department), 6 wt% SFG-6 synthetic flake graphite (Timcal Ltd., Graphites and Technologies), and 6 wt% acetylene black. Electrodes were cast as a slurry in 1-methyl-2-pyrrolidinone (Sigma Aldrich, 99%) onto aluminum current collectors and dried for 24 hours in air followed by 12-24 hours in a vacuum oven at 120 °C. Cathodes with an area of 1.8 cm^2 were punched from the cast electrode and typically had loadings of about 1 mAh/cm^2. Assembly of lithium half-cells in 2032 coin cells was performed in a helium filled glove box using 1 M $LiPF_6$ in 1:2 ethylene carbonate/dimethylcarbonate (EC/DMC) electrolyte solution and a Celgard 3401 separator. At least two cells of the same type were tested for each material to ensure reproducibility. Electrochemical studies were undertaken galvanostatically using an Arbin BT/HSP-2043 and/or a Macpile II (Bio-Logic, S.A., Claix, France) automated

cycling data recorder between 2.0 and 3.9 V at room temperature. Cells were always charged at a current density corresponding to C/25 and allowed to rest 15 minutes between half-cycles.

Results and Discussion

All powders were determined to be phase-pure by XRD analysis. The primary particle sizes found in the powders of all samples were highly variable, ranging from <100 nm to more than 1 μm. Agglomerates were larger than 2 μm in all cases, with large, bimodal size distributions observed in both the particle size and SEM studies. Individual particle morphologies varied widely as well, ranging from large smooth platelets to highly porous particles, which formed due to gas evolution during synthesis (Figure 1).

Our previous work[18] showed that some organic or polymeric precursors used to produce carbon coatings did not decompose completely at the low synthesis temperatures used to make $LiFePO_4$. Residual hydrogen and functional groups on carbon lower the electronic conductivity, resulting in electrode materials with poor electrochemical performance. Of the additives examined in Reference 18, PA (pyromellitic acid or 1, 2, 4, 5-benzenetetracarboxylic acid) gave the best results, as it was found to decompose readily and resulted in a high quality carbon coating. To examine the effect of varying the amount of PA on the carbon amount and structure in the final product, several samples were prepared for the current study. There is usually a small amount of residual (*in situ*) carbon even in materials prepared without additives, due to the decomposition of organic moieties in the reactants. This amount varies with processing temperature and other variables, and was 0.3% under the conditions used here. The addition of PA during synthesis results in a modest increase in the carbon content (Table 1) and a general decrease in the H/C ratio with

some sample variation, close to that of PA itself (0.05). The latter indicates the degree of decomposition of the organic components in the synthesis mixture, and suggests that better quality carbons are produced from the additive, due, in part, to its lower hydrogen content. Also included in Table 1 are carbon structural parameters determined from analysis of the Raman spectra obtained on the various $LiFePO_4$ samples.

Raman spectroscopy is a particularly useful tool for characterizing the near-surface structure (i.e. disorder and crystallite formation) of carbon films because carbon is a relatively strong scatterer with two E_{2g} modes predicted to be Raman active. Figure 2a shows a typical Raman spectrum of a $LiFePO_4$ powder from this study. A sharp band at 953 cm^{-1} corresponds to the symmetric A_g mode (ν_1), whereas the two weaker bands at 997 and 1098 cm^{-1} are attributed to the asymmetric stretching modes (ν_3) of the $(PO_4)^{3-}$ anion.[19] Two intense broad bands located at ~1350 and 1593 cm^{-1} are assigned to the D and G bands of the residual carbon, respectively. The relative peak heights and widths of carbon bands change substantially with the pyrolysis temperature and the nature of the precursor materials. The variation of the width and intensity of the D and G bands is related to the growth and size of different carbon phases, the presence of functional groups and impurities. While most authors agree that the peak at 1590 cm^{-1} is the first order scattering from the in-plane E_{2g} mode, there are notable discrepancies in the frequency of this peak reported in the literature, depending on the type of carbon and preparation method. The G band tends to broaden and shift toward higher frequencies with decreasing intraplanar (*La*) and interplanar (*Lc*) microcrystallite dimensions. This effect has been also explained in terms of the superposition of the G band and a new D` band at ~1620 cm^{-1}, which originates from sp^2 carbon vibrations. When *La* and *Lc* decrease, a new feature at 1360

cm^{-1}, the D band, is usually observed. The origin of this band has been the subject of many controversies. It is usually assigned to the A_{1g} mode that is associated with the breakage of symmetry occurring at the edges of graphite sheets.[20, 21]

To resolve the Raman spectra of the residual carbon in the $LiFePO_4$ samples, we applied a standard peak deconvolution procedure after a polynomial background subtraction. Figure 2b shows a Raman spectrum of the residual carbon that was resolved into individual bands. A deconvolution of the Raman spectrum of all of the $LiFePO_4$ samples using a fit with two carbon D and G lines did not give accurate results. Four Gaussian bands were necessary to account for the observed Raman features with minimum error. Those bands are situated at ~1190, 1350, 1518 and 1590 cm^{-1}. The bands at ~1518 cm^{-1} and 1190 cm^{-1} have uncertain origins but they have already been observed in disordered carbon black and diamond like carbons.[22,23] That could imply that short-range vibrations of sp^3 coordinated carbons contribute to the disordered spectra. As a matter of fact, carbons produced at ~700^oC usually contain a significant amount of disorganized or, in other words, truly amorphous phase. Coordination of carbon atoms in this short-order phase is highly random and varies from sp^2 and sp^3 but there are no long-order graphite- and diamond-like domains in it. Numerous HRTEM studies of carbon blacks reveal that the bulk of carbon black particles consist of a completely disorganized carbon structure whereas small (10-40 Å) graphene domains are arranged at the surface. The ratio between the "disorganized" poorly conductive phase and graphite-like phase in carbon blacks is very dependent on the pyrolysis temperature and the type of organic precursor. It is the main reason why Raman spectra of "amorphous carbons" cannot be fit with two Gaussian bands. It is also reflected by the strong temperature dependence of electronic conductivity of

pyrolyzed carbon blacks. The appearance of strong sp^2 related Raman modes, and the absence of a sharp characteristic 1330 cm^{-1} diamond Raman peak in the visible Raman spectra lead to the suggestion that these pyrolyzed carbons are amorphous with a predominant sp^2 fraction.[24] However, other studies substantiated that diamond-like and/or amorphous carbons can contain a significant fraction of sp^3 bonds while the sp^2 component might be very small.[25] Raman spectroscopy is mainly sensitive to the configuration of sp^2 sites because of their higher cross section. A multi-wavelength analysis is always recommended to give reliable qualitative information about sp^2/sp^2-coordinated carbon ratios.

The D/G (disordered/graphene) and sp^2/sp^3 ratios determined in this study by the analysis of the Raman spectra (Table 1) do not yield the actual ratios but rather values that are correlated to these structural parameters. Thus, they are useful for comparing samples to each other but not as quantitative measures of the graphene or sp^3 contents. Based on this analysis, the data in Table 1 show that D/G ratios decrease and sp^2/sp3 ratios increase as more PA is added, up to about 6 wt. %. Thus, the structure of carbon produced when PA is present during calcination is markedly different from that produced from the precursors alone.

Pressed pellet conductivities as a function of temperature were obtained for several of these materials (Figure 3). The room temperature conductivity of ~10^{-8} S/cm extrapolated from the Arrhenius fit for the $LiFePO_4$ powder produced without PA agrees well with data previously obtained on pure $LiFePO_4$ powders,[26] despite the presence of 0.3% residual carbon from the reaction precursors. Samples prepared with 4 or 6 wt. % PA have room temperature conductivities nearly two orders of magnitude higher, although the

carbon contents are increased to only about 0.7 wt. %. Further improvements are observed when 8% PA is used.

Figure 4 shows the capacities obtained at several discharge rates for lithium cells containing materials processed with PA and the corresponding D/G ratios. The carbon structural parameters and pressed pellet conductivities correlate well with electrochemical performance. The structure of the carbon affects the conductivity of the composite material, which also influences the rate behavior in electrochemical cells. Thus, the latter tends to track the former. The differences seen in the conductivities and electrochemical characteristics of the samples prepared with larger amounts of PA primarily shows the influence of increasing the carbon amount, as the carbon structure does not vary significantly. It is, however, interesting to note that materials previously described in reference 18, having similar carbon contents and particle morphologies, perform worse than those presented in Figure 4. For example, compare sample 7SG, prepared without additives, and containing 0.7 wt. % C, to that of the material processed with 6 wt. % PA having 0.76 wt. % C in the current work. The former delivers less than 100 mAh/g at C/25 while the latter gives 120 mAh/g.

While the improvement in carbon structure, pressed pellet conductivities and electrochemical performance seen in samples prepared with PA is striking, rate limitations are still evident. Improvements in the carbon structure and/or increases in the carbon content are still necessary for optimum performance.

There is considerable precedence in the carbon literature for the use of transition metal-containing compounds as low temperature (500-1000° C) catalysts for the production of graphitic carbon structures. In particular, iron nitrate,[27] ferrocene,[28, 29] and ferrocene

derivatives[30] have been used extensively under conditions very similar to those used for the synthesis of $LiFePO_4$. In the case of iron nitrate catalysts, progressively more reduced iron oxides are formed during heating in a hydrocarbon rich, oxygen-controlled environment.[27] This process eventually leads to the formation of iron carbide, which acts as a nucleation site for graphite. Furthermore, the role of iron oxides in the graphitization process may explain the variability of the carbon produced in the sol-gel samples made without additives in references 17 and 18, as these are common impurities in $LiFePO_4$ preparations.

Samples calcined with small amounts of iron nitrate (0.001-0.01 wt. %) and PA gave powders with C contents below 1 wt. %, similar to those calcined with PA alone (Table 1). While the D/G ratios are not significantly changed from those of samples processed with similar amounts of PA, sp^2/sp^3 ratios are higher. This suggests that, while the graphene domain sizes are not changed from materials prepared with PA only, there is a greater proportion of carbon with a graphitic nature. It is possible to assess the effect of the increased sp^2 character on the electronic conductivity by comparing the results for two composites with identical carbon contents (0.71%), one processed with iron nitrate, and one without, in Figure 3. The former gives better electrochemical performance than the latter (Figure 5). The higher discharge capacities at given rates can be attributed to the increased composite conductivity ($\sim 10^{-5}$ S/cm at room temperature) due to the higher sp^2/sp^3 ratio. The conductivity of this sample exceeds that of all non-catalyst treated samples except the one made with 8 wt. % PA, which contains more carbon. Note also that the effect of a higher sp^2/sp^3 ratio can compensate for a lower carbon content in terms of electrochemical performance; in Figure 5, a $LiFePO_4$ material containing only 0.59% C (processed with

both PA and iron nitrate) is superior to the one containing 0.71% C, (processed with only PA) which has a lower sp^2/sp^3 ratio.

$LiFePO_4$ processed with PA and higher concentrations of iron nitrate performed worse than the materials made with 0.01% iron nitrate or less listed in Table 1. For graphitization to occur, iron nitrate (or the oxides that form from thermal decomposition) must be located in carbon-rich areas on the surfaces of the powders. Excessive iron nitrate results in an overabundance of resistive iron oxide, which adversely affects the electrochemical performance. Conversely, carbon-rich areas not in contact with the catalyst will not graphitize at the relatively low temperatures used to synthesis $LiFePO_4$. A low concentration of iron nitrate is preferable to prevent excessive formation of iron oxide, but it must be dispersed homogenously with the carbon source for ideal results. For some materials processed with PA and iron nitrate, considerable spot-to-spot variation in the Raman spectra were observed, indicating that the quality of the carbon was not uniform throughout the powder. Consequently, these materials did not show any appreciable improvement in the electrochemical performance and are not further considered here.

Ferrocene and its derivatives have advantages over iron nitrate as they contain both catalyst centers and carbon sources within the same molecules, which overcome difficulties in ensuring close contact between the two entities. They have been used extensively in the synthesis of nano-structured carbon materials,[28, 29, 30] and as soot control agents for cleaner burning fuels.[31] A composite prepared with 1 wt. % ferrocene, however, has a low carbon content (Table 1), only slightly higher than that of $LiFePO_4$ prepared without any additives. Ferrocene sublimes at about 175°C,[32] so much of it is lost during calcination under the conditions used here. The quality of carbon is poor, judging from the structural factors

listed in Table 1, although its thorough decomposition is evidenced by a low H/C ratio. In contrast, $LiFePO_4$ prepared with either ferrocene or FCA as well as PA has significantly higher carbon contents than materials prepared with the same amount of PA alone (Table 1), although the final amount is still less than 2 wt. %. This suggests an interaction between the ferrocene and PA occurs upon heating, which results in improved retention of elemental carbon. The H/C ratios of these composites are lower than that of the starting materials, ferrocene (0.08) and FCA (0.075) themselves, indicating nearly complete thermal decomposition. The carbon structural factors, as determined by Raman spectroscopy, are similar to that of composites made with PA alone, although the sp^2/sp^3 ratios are less than that of the materials processed with iron nitrate. Thus, the several orders of magnitude increase in conductivity of a ferrocene/PA-treated $LiFePO_4$ pressed pellet compared to the others in Figure 3, is mainly attributable to the increase in carbon content, rather than to any improvements in carbon structure over composites made with PA alone.

Additional peaks at low wave numbers were observed in the Raman spectra of several samples processed with ferrocene and PA (Figure 6), some of which match those reported for Fe_3C.[33,34,35] A similar Raman spectrum is observed for the thermal decomposition products of ferrocene alone in a sealed tube, under conditions much like those used to produce $LiFePO_4$ in this study. In addition to Fe_3C and other forms of carbon, numerous carbon nanotubes with diameters of about 5 nm were observed in the transmission electron micrographs of the ferrocene thermal decomposition products.[36] Ferrocene is commonly used as a catalyst precursor for the production of either single-walled[31] or multi-walled[37, 38] carbon nanotubes at moderate temperatures. Deposition of nanotubes (and the related process of metal dusting corrosion) takes place via the

intermediate Fe_3C,[39] which is formed as carbon diffuses through the metal nanoparticles formed during decomposition.

The presence of Fe_3C and, possibly, carbon nanotubes in some of the ferrocene/PA-treated $LiFePO_4$ composites complicates the interpretation of the Raman spectra, as some of the peaks overlap with the D and G bands of carbon itself. Additionally, Fe_3C is metallic and even small amounts can be expected to influence the pressed pellet conductivities. For these reasons, these samples have been omitted from the present discussion, although they will be the subjects of a future publication.

Figure 7 shows the specific capacity as a function of current density for lithium cells containing $LiFePO_4$ samples treated with ferrocene or FCA and PA. Results for a cell containing material treated with ferrocene alone and another with PA alone are also included, for comparison. The best high rate behavior seen in this study was obtained for cells containing $LiFePO_4$ processed with 1 wt. % ferrocene and 6 wt. % PA, in accordance with the high pressed pellet conductivities seen in Figure 3. Because the structural characteristics of the carbon do not vary much for these samples (with the exception of the poorly performing material treated with ferrocene alone), the differences in the electrochemical performance shown in Figure 7 can be attributed mainly to the changes in carbon content. The material containing 1.56% carbon (processed with FCA and PA), however, performs somewhat worse at C-rate than the one treated with ferrocene and PA, which has a marginally lower carbon content of 1.45% and slightly lower pressed pellet conductivities. As with some of the materials calcined with iron nitrate, considerable spot-to-spot variation was seen in the Raman spectra of the FCA-treated material, indicating non-homogeneity of the carbon coating. (The structural factors in Table 1 derived from

these spectra are averages taken from 10 spectra). The non-homogeneity is less likely to have an impact on pressed pellet conductivities, in which a percolation threshold is easier to achieve, than in a porous composite electrode containing the same material, used to obtain the electrochemical data. In contrast, much better homogeneity in the Raman spectra was observed for materials processed with ferrocene. FCA does not sublime like ferrocene does, but undergoes a two-step thermal decomposition at 250°C and 410°C.[32] The volatility of ferrocene may be beneficial in that it promotes a more even distribution of carbon compared to FCA. A recent transmission electron microscopy study of $LiFePO_4$ treated with 6% PA and 1% ferrocene showed that carbon is located on all the surfaces of primary particles, even those fused into agglomerates like those shown in Figure 1.[40]

The results presented here show that the composite conductivity, and therefore, the electrochemical performance, is related to the amount, structure, and distribution of the carbon in the coatings on the $LiFePO_4$ particles. In some cases, composites containing less carbon are more conductive than those with more, due to a higher sp^2 character. This translates directly into improved electrochemical performance. The best results in this study, however, were obtained for composites with carbon contents above 1 wt. %. This may be due, in part, to the fact that it is easier to obtain complete coverage over particle surfaces when more carbon is present. Provided that a relatively homogeneous coating can be produced by, for example, better mixing prior to calcination, what is the lowest carbon content needed to produce a high-rate $LiFePO_4$? How much improvement in the carbon structure is necessary to allow a substantial decrease in the content? The pressed pellet conductivity data, although fairly limited, offers some insights into these questions. In Figure 8, the logs of the room temperature pressed pellet conductivities of three samples

with similar carbon contents (~0.7 wt. %) are plotted vs. the sp^2/sp^3 ratios. D/G and H/C ratios of the carbons in these composites are fairly similar, so that the data mainly show the effect of increasing the sp^2 character. Data for two other materials with higher carbon contents (~1.5 wt. %) are also plotted; these points fall on a line roughly parallel to the low-carbon sample line. Presumably, conductivity data for samples with intermediate carbon contents would fall on other parallels between these two lines, provided that the details of coverage were similar and the other structural characteristics of the carbons were not significantly different than for these two sets of samples. The dotted tie lines show that an sp^2/sp^3 ratio close to 0.45 (i.e., requiring more than double the sp^2 character) is needed for ~0.7 wt. %C carbon composites to achieve conductivities (and, by inference, electrochemical performances) similar to that of $LiFePO_4$ composites with ~1.5 wt. % carbon in them.

An alternative approach is presented in Figure 9. Here, $LiFePO_4$/C composite conductivities are calculated using an equation derived from the simple bricklayer model described by Maier.[41] In this model, mono-sized cubic grains of the major phase having a bulk conductivity, σ_{bulk}, are considered to be uniformly surrounded by a secondary grain boundary phase with conductivities defined in the parallel ($\sigma_{gb}^{\parallel}$) and perpendicular ($\sigma_{gb}^{\perp}$) directions. For a situation where the secondary phase is more conductive than the bulk and the thickness of the grain boundary (δ_{gb}) is much smaller than that of grains in the bulk (d_{grain}), $\sigma_{gb}^{\perp}$ can be ignored, and the measured composite conductivity (σ_m) is: [42]

$$\sigma_m = \left(1 + \frac{\sigma_{gb}^{\parallel}}{\sigma_{bulk}} \frac{\delta_{gb}}{d_{grain}}\right)\sigma_{bulk} \quad (1)$$

For $\sigma_{bulk} = 10^{-9}$ S/cm, the curves shown in Figure 9, showing the effect of varying the grain boundary conductivity and thickness of the carbon layer, are produced. An 'x' marks the estimated grain boundary conductivity of about 0.1 S/cm for the $LiFePO_4$ sample processed with 1% ferrocene and 6% PA (1.45 wt. % C), using the room temperature composite conductivity data from Figure 3 and estimating an average δ_{gb} of 5 nm and grain size, d_{grain}, of 200 nm from the TEM results. [40]

The samples in this study deviate markedly from the ideal of mono-sized grains evenly coated with a secondary phase, necessitating considerable caution[43] when attempting to determine the carbon coating conductivities using this model. Still, a careful examination of the composite conductivity behavior as a function of carbon coating thickness in an ideal system is instructive for the purpose of designing high-rate $LiFePO_4$ electrodes. It is clear that increasing the carbon amount (or decreasing the grain size) has the greatest effect on composite conductivities at low values of δ_{gb}/d_{grain}, and improves most dramatically when $\sigma_{gb}^{II}/\sigma_{bulk} > 10^3$. Increasing the coating thickness past a certain point results in rapidly diminishing returns, especially if it is poorly conducting. It is much more effective to improve the grain boundary conductivity instead. The strategies employed in this study may be used to achieve this goal.

Conclusions

Several synthetic additives were used to improve the carbon coatings on $LiFePO_4$ electrode materials. PA added prior to calcination decreases the D/G ratios of the carbon produced *in situ*, while the use of both iron nitrate and PA results in increased sp^2 character without further improving D/G ratios. Thus, a greater fraction of the carbon has graphitic character

although domain sizes are not increased. The production of more graphitic carbon coatings results in higher pressed pellet conductivities of the $LiFePO_4$/C composites and improved electrochemical performance of cells containing these materials, although the carbon content is not necessarily increased. The combination of both ferrocene and PA used during $LiFePO_4$ synthesis causes more carbon to be retained, although the structural characteristics are similar to that produced from the same amount of PA alone.

Acknowledgment

This work was supported by the Assistant Secretary for Energy Efficiency and Renewable Energy, Office of FreedomCAR and Vehicle Technologies of the U.S. Department of Energy under contract no. DE-AC02-05CH11231.

References

1. A. K. Padhi, K. S. Nanjundaswamy, J. B. Goodenough, *J. Electrochem. Soc.,* **144**, 1189 (1997).

2. A. S. Andersson, B. Kalska, L. Haggstrom, J. O. Thomas, *Solid State Ionics*, **130**, 41 (2000).

3. S. Shi, L. Liu, C. Ouyang, D.-S. Wang, Z. Wang, L. Chen, X. Huang, *Physical Review B*, **68**, 195108 (2003).

4. F. Croce, A. D'Epifanio, J. Hassoun, A. Deptula, T. Olezac, B. Scrosati, *Electrochem. Solid-State Lett.*, **5**, A47 (2002).

5. A. Yamada, S. C. Chung, K. Hinokuma, *J. Electrochem. Soc.*, **148**, A224 (2001).

6. M. Takahashi, S. Tobishima, K. Takei, Y. Sakurai, *J. Power Sources*, **97-98**, 508 (2001).

7. P. P. Prosini, M. Carewska, S. Scaccia, P. Wisniewski, S. Passerini, M. Pasquali, *J. Electrochem. Soc.*, **149**, A886 (2002).

8. R. Dominko, J. M. Goupil, M. Bele, M. Gaberscek, M. Remskar, D. Hanzel, J. Jamnik, *J. Electrochem. Soc.*, **152**, A858 (2005).

9. S.-Y. Chung, J. T. Bloking, Y.-M. Chiang, *Nat. Mater.* **1**, 123 (2002).

10. P. Subramanya Herle, B. Ellis, N. Coombs, L.F. Nazar, *Nat. Mat.*, **3**, 147 (2004).

11. C. Wurm, M. Morcette, S. Gwizdala, C. Masquelier, World Pat. WO 02/099913 A1 (2002).

12. N. Ravet, Y. Chouinard, J.F. Magnan, S. Besner, M. Gauthier, M. Armand, *J. Power Sources*, **97-99**, 503 (2001).

13. H. Huang, S.-C. Yin, L. F. Nazar, *Electrochem. Solid-State Lett.*, **4**, A170 (2001).

14. M.M. Doeff, J. Wilcox, R. Kostecki, G. Lau, *J. Power Sources*, in press.

15. S.L. Bewlay, K. Konstantinov, G.X. Wang, S.X. Dou, H.K. Liu, *Materials Letters*, **58**, 1788 (2004).

16. Z. Chen, J. R. Dahn, *J. Electrochem. Soc.*, **149**, A1184 (2002).

17. M.M. Doeff, Y. Hu, F. McLarnon, R. Kostecki, *Electrochem. Solid-State Lett.*, **6**, A207 (2003).

18. Y. Hu, M. M. Doeff, R. Kostecki, and R. Fiñones, *J. Electrochem. Soc.*, **151**, A1279 (2004).

19. C. B. Burba and R. Frech, *J. Electrochem. Soc.*, **151**, A1032 (2004).

20. M. J. Matthews, M.A. Pimenta, G. Dresselhaus, M. S. Dresselhaus, and M. Endo, *Phys. Rev. B,* **59**, 6585 (1999).

21. C. Thomsen and S. Reich, *Phys. Rev. Lett.,* **85**, 5214 (2000).

22. J. N. Rouzaud and A. Oberlin, *Thin Solid Films,* **105**, 75 (1983).

23. F. Bonhomme, J. C. Lassegues, L. Servant, *J. Electrochem. Soc.*, **148,** E450 (2001)

24. Ait Salah, A. Mauger, K. Zaghib, J. B. Goodenough, N. Ravet, M. Gauthier, F. Gendron, C. M. Julien, *J. Electrochem. Soc.*, **153** A1692 (2006).

25. C. Casiraghi, A. C. Ferrari, J. Robertson, *Phys. Rev B,* **72**, 085401 (2005) and references therein.

26. S. Shi, L. Liu, C. Ouyang, D-S. Wang, Z. Wang, L. Chen, and X. Huan, *Phys. Rev. B*, **68**, 195108 (2003).

27. C. Emmenegger, J.-M. Bonard, P. Mauron, P. Sudan, A. Lepora, B. Grobety, A. Zuttel, L. Schlapbach, *Carbon*, **41**, 539 (2003).

28. K. Kuwana, K. Saito, *Carbon*, **43**, 2088 (2005).

29. S. Liu, R.J. Wehmschulte, *Carbon*, **43**, 1550 (2005).

30. T.M. Keller, Qadri, S.B., *Chem. Mater.*, **16**, 1091 (2004).

31. R. L. Vander Wal and L. J. Hall, *Combust. Flame*, **130**, 27 (2002).

32 A. C. de Souza, A. T. N. Pires, and V. Soldi, *J. Therm. Anal. and Calor.*, **70,** 405 (2002).

33. C. T. Lee, M. S. Odziemkowski, and D. W. Shoesmith, *J. Electrochem. Soc.*, **153,** B33 (2006).

34. X.-X. Bi, B. Ganguly, G.P. Huffman, F.E. Huggins, M. Endo, and P.C. Eklund, *J. Mater. Res.,* **8**, 1666 (1993).

35. P.L. Stanghellini, M. J. Sailor, P. Kuznefos, K. H. Whitmire, J. A. Hriljac, J. W. Kolis, Y. Zheng, and D. G. Shriver, *Inorg. Chem.* **26**, 2950 (1987).

36. J. D. Wilcox and M. M. Doeff, unpublished results.

37. R. Andrews, D. Jacques, A. M. Rao, F. Derbyshire, D. Qian, X. Fan, E. C. Dickey, and J. Chen, *Chem. Phys. Lett.*, **303**, 467 (1999).

38. Y T. Lee, N. S. Kim, J. Park, J. B. Han, Y. S. Choi, H. Ryu, H. J. Lee, *Chem. Phys. Lett.,* **372,** 853 (2003).

39. Z. Zeng and K. Natesan, *Chem. Mater.*, **17**, 3794 (2005).

40. H. Gabrisch, J. D. Wilcox, and M. M. Doeff, *Electrochem. and Sol. State Lett.*, **9** A360 (2006).

41. J. Maier, *Sol. State Ionics*, **157**, 327 (2003).

42. X. Guo and Y. Ding, *J. Electrochem. Soc.*, **151**, J1 (2004).

43. J. Fleig, *Solid State Ionics,* **131,** 117 (2000).

Table 1. Carbon contents, H/C ratios, D/G and sp^2/sp^3 ratios for selected $LiFePO_4$ samples processed with pyromellitic acid (PA), with or without graphitization catalysts as noted.

Wt.% PA	*Catalyst*	*% C*	*H/C*	*Average D/G (S.D.)* [a]	*sp^2/sp^3 (S. D.)*[b]
0	—	0.304	0.079	1.26 (0.013)	0.091 (0.0298)
2	—	0.423	0.048	1.19 (0.029)	0.120 (0.0996)
4	—	0.714	0.045	1.12 (0.005)	0.257 (0.004)
6	—	0.764	0.054	1.10 (0.059)	0.271 (0.061)
8	—	0.843	0.037	1.11 (0.243)	0.243 (0.016)
6	0.001 wt. % $Fe(NO_3)_3$	0.711	0.056	1.11 (0.018)	0.319 (0.011)
6	0.01 wt. % $Fe(NO_3)_3$	0.594	0.056	1.06 (0.052)	0.309 (0.091)
0	1 wt % ferrocene	0.551	0.039	1.98 (0.056)	0.0067 (0.0049)
6	1 wt. % ferrocene	1.45	0.044	1.09 (0.040)	0.183 (0.053)
6	1 wt. % FCA[c]	1.56	0.028	1.11 (0.009)	0.204 (0.009)

a) S.D.= standard deviation. Values are relative measures obtained from analysis of Raman spectra. See text for explanation of how these were obtained.

b) S.D.=standard deviation. Values are relative measures obtained from analysis of Raman spectra. See text for explanation of how these were obtained.

c) FCA=ferrocenecarboxylic acid.

Figure Captions.

Figure 1. Scanning electron micrograph of a typical $LiFePO_4$/C composite.

Figure 2. A typical Raman spectrum of a $LiFePO_4$ powder (a). The Raman spectrum of the residual carbon is resolved into four bands (b), as described in the text.

Figure 3. Pressed pellet conductivities as a function of temperature for several of the $LiFePO_4$/C materials prepared for this study.

Figure 4. Specific capacities obtained at various discharge rates for lithium cells containing $LiFePO_4$ samples prepared with and without PA (left axis), and D/G ratios as determined by Raman microprobe spectroscopy for the same samples (right axis).

Figure 5. Specific capacities as a function of discharge rate for lithium cells containing three different samples of $LiFePO_4$, one processed with 4% PA alone, one with 0.001 wt. % iron nitrate and 6 wt. % PA, and one with 8% PA and 0.01% iron nitrate.

Figure 6. Raman spectra taken on several spots of a $LiFePO_4$ powder processed with 1/2% ferrocene and 6% PA (this sample is not included in Table 1). The top and bottom spectrum show the normal peaks attributable to $LiFePO_4$ and carbon (see text). In the middle spectrum, peaks from iron carbide overlap the D-band of carbon. Iron carbide and carbon nanotube peaks also appear at low wavenumbers.

Figure 7. Specific capacities as a function of discharge rate for lithium cells containing $LiFePO_4$ samples processed with ferrocene or FCA, with or without PA, as noted.

Figure 8. Pressed pellet conductivities as a function of sp^2/sp^3 ratio for two different sets of composite $LiFePO_4$ samples having similar carbon contents. The solid gray line shows a linear fit to the data for composites with 0.71-0.76 wt. % carbon. The dashed gray line parallels this fit and connects the data for composites with higher carbon contents. Dotted black lines show the improvement needed in sp^2/sp^3 ratio in the low carbon samples to achieve conductivities similar to those found in the high carbon samples. FC=ferrocene and other abbreviations are as explained in the text.

Figure 9. Relationship between composite conductivities and volume fraction of carbon for given coating conductivities, calculated using the bricklayer model, as described in the text. The bulk conductivity of $LiFePO_4$ was taken as 10^{-9} S/cm for the calculations. The point marked with an 'x' indicates the estimated composite conductivity for a sample processed with 6% PA and 1% ferrocene, containing 1.45 wt. % carbon, based on data from Figure 3 and reference 40.

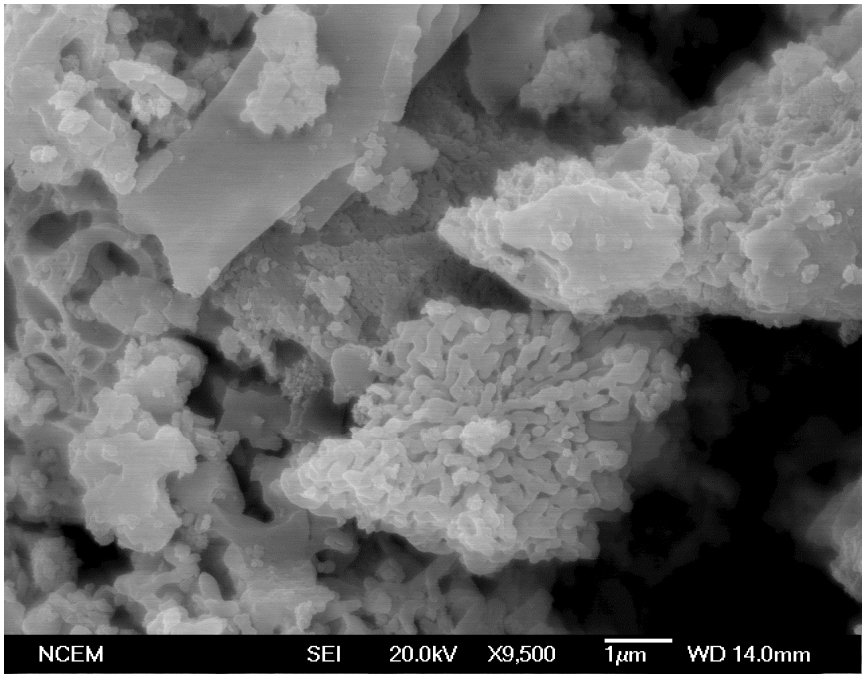

Figure 1

a)

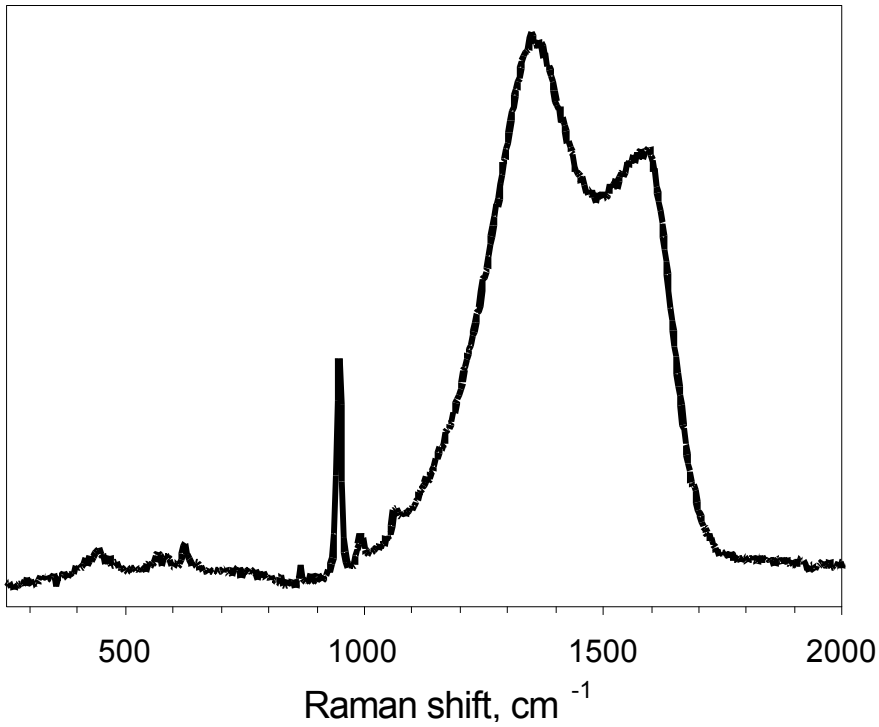
500
1000
1500
2000
Raman shift, cm -1

b)

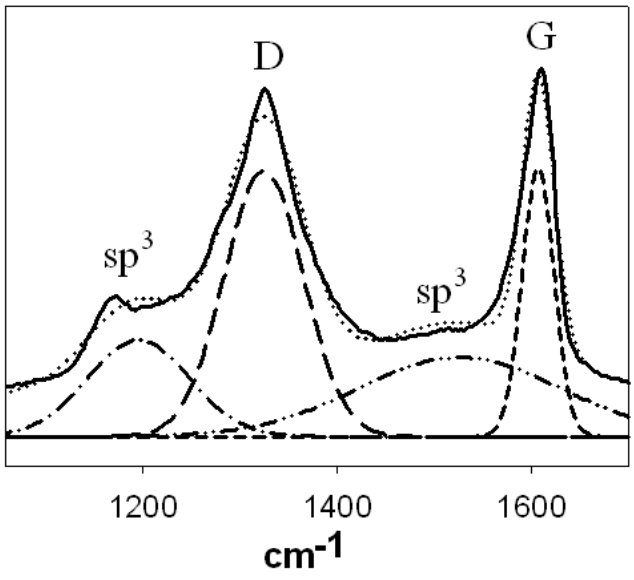
D
G
sp3
sp3
1200
1400
1600
cm-1

Figure 2

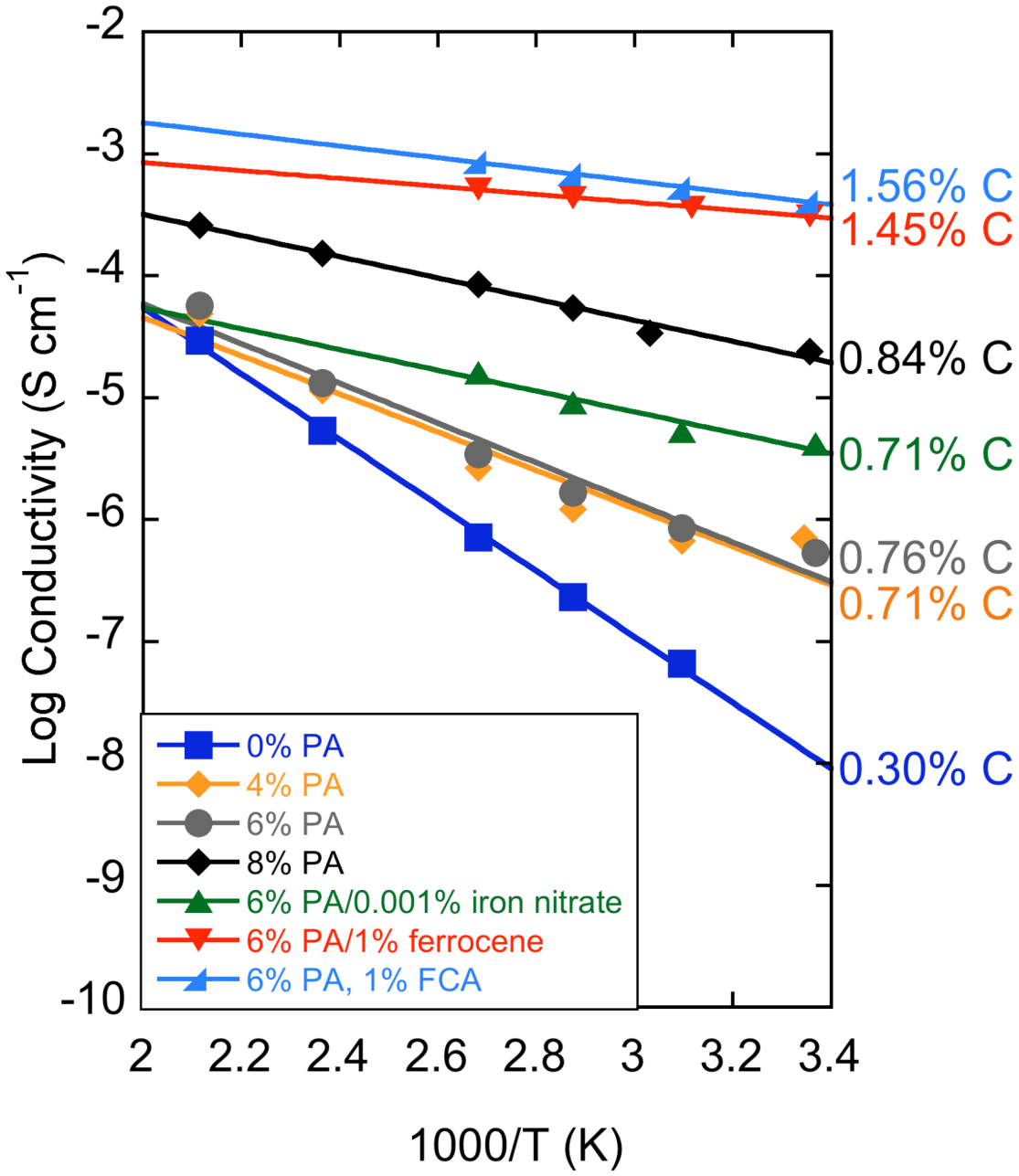
-2
-3
-4
-5
-6
-7
-8
-9
-10
Log Conductivity (S cm-1)
2
2.2
2.4
2.6
2.8
3
3.2
3.4
1000/T (K)
0% PA
4% PA
6% PA
8% PA
6% PA/0.001% iron nitrate
6% PA/1% ferrocene
6% PA, 1% FCA
1.56% C
1.45% C
0.84% C
0.71% C
0.76% C
0.71% C
0.30% C

Figure 3.

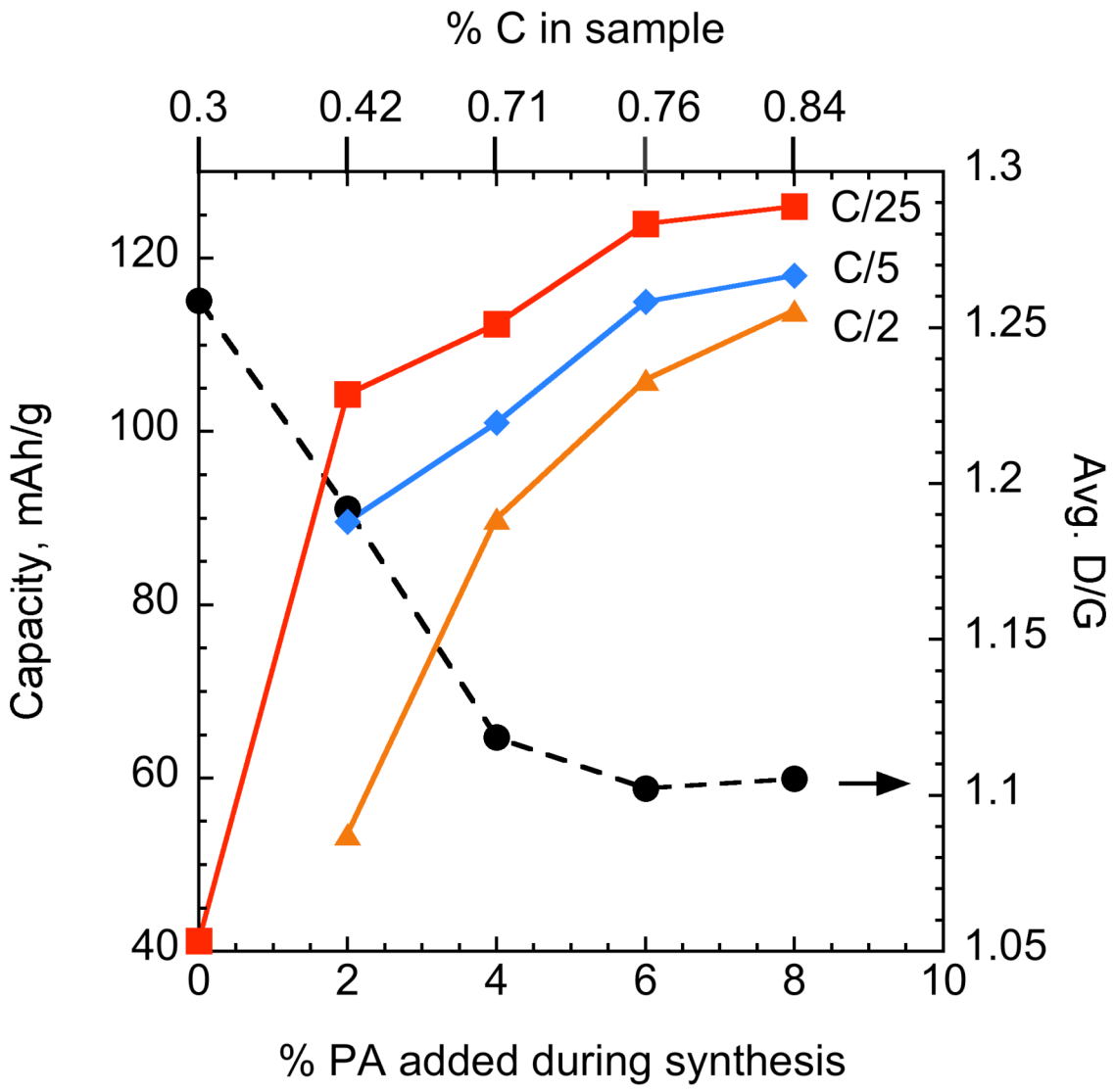
% C in sample
0.3
0.42
0.71
0.76
0.84
C/25
C/5
C/2
Capacity, mAh/g
Avg. D/G
% PA added during synthesis
120
100
80
60
40
1.3
1.25
1.2
1.15
1.1
1.05
0
2
4
6
8
10

Figure 4

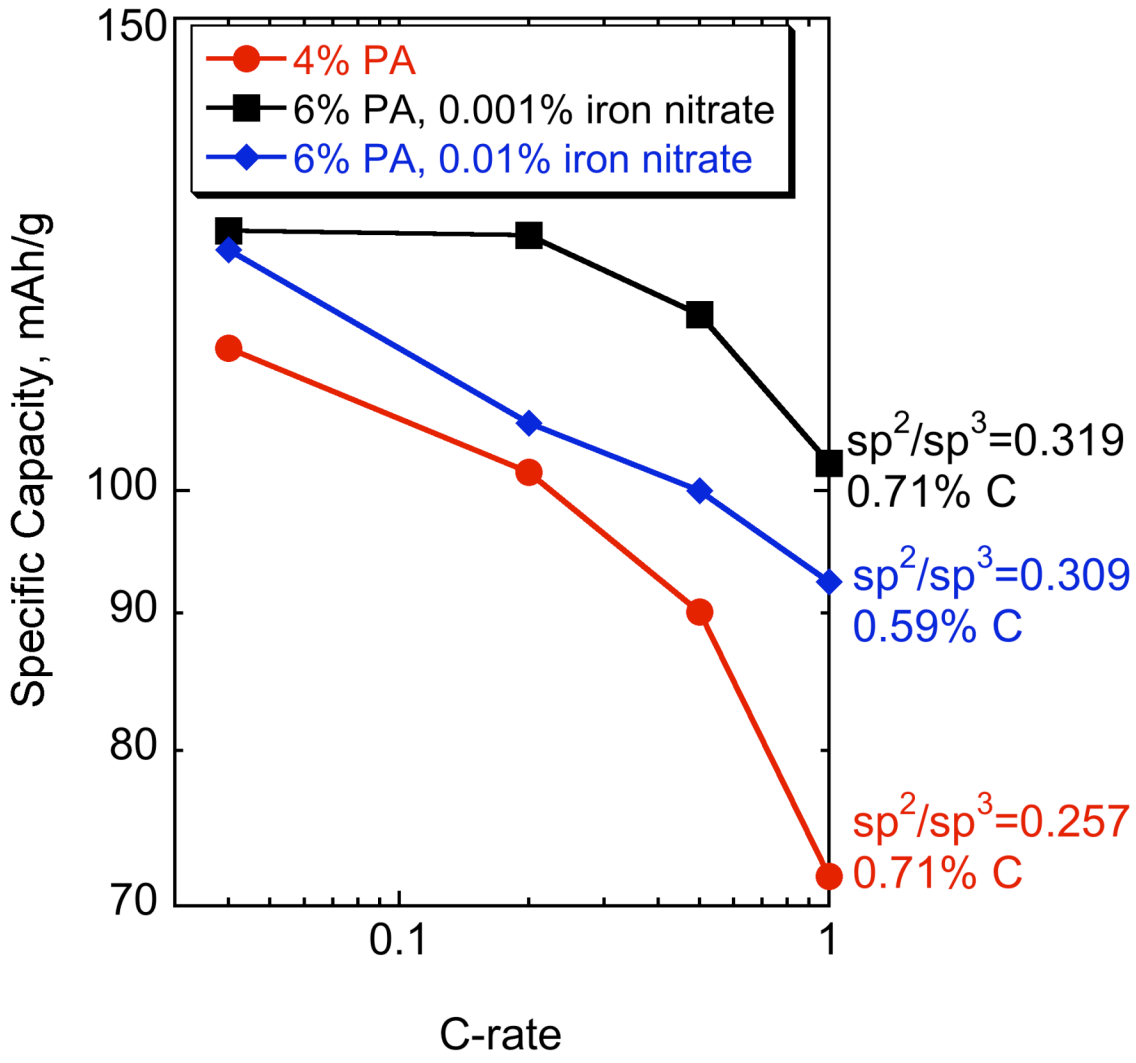
150
100
90
80
70
0.1
1
C-rate
Specific Capacity, mAh/g
4% PA
6% PA, 0.001% iron nitrate
6% PA, 0.01% iron nitrate
sp2/sp3=0.319
0.71% C
sp2/sp3=0.309
0.59% C
sp2/sp3=0.257
0.71% C

Figure 5

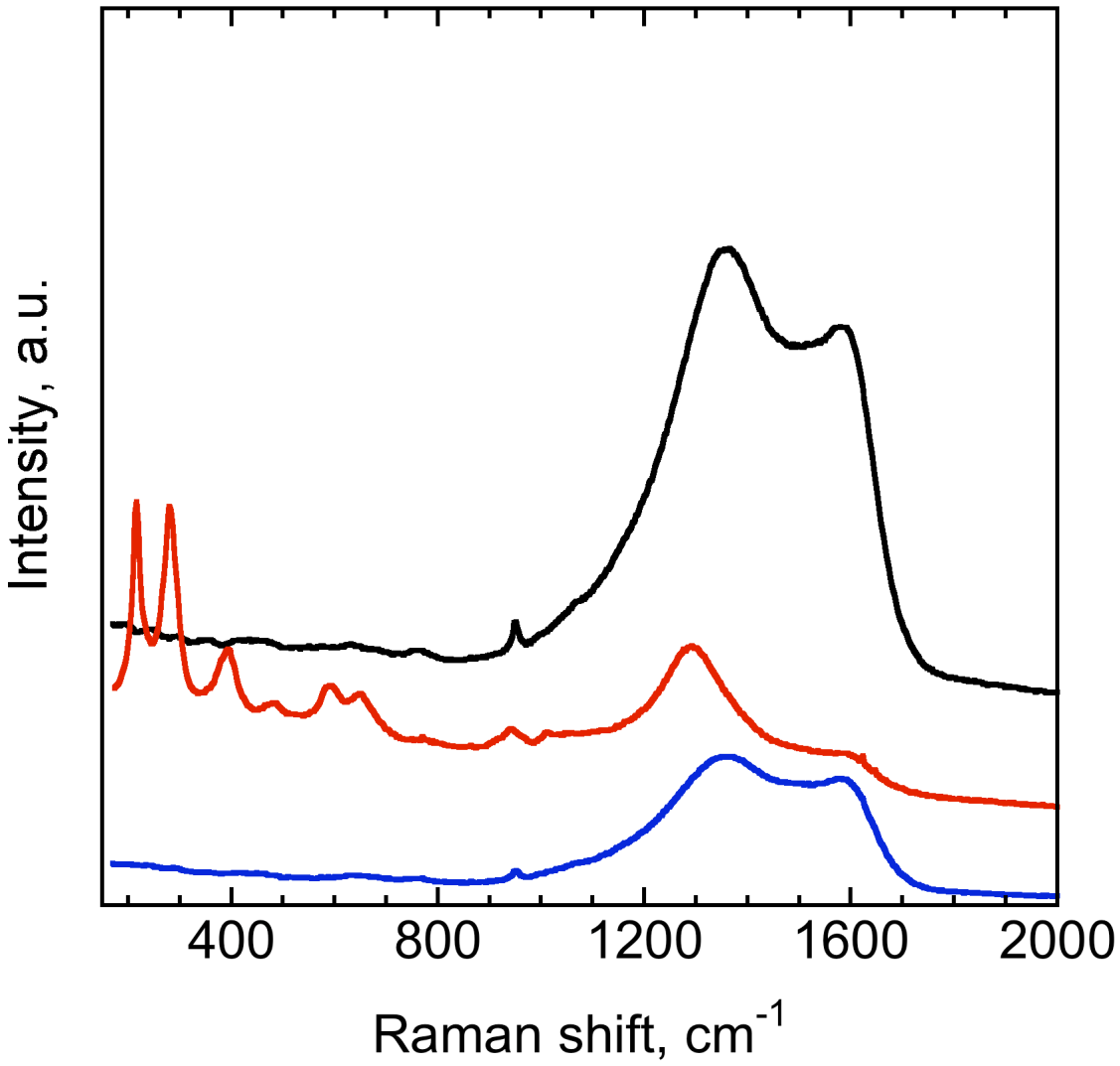

Figure 6

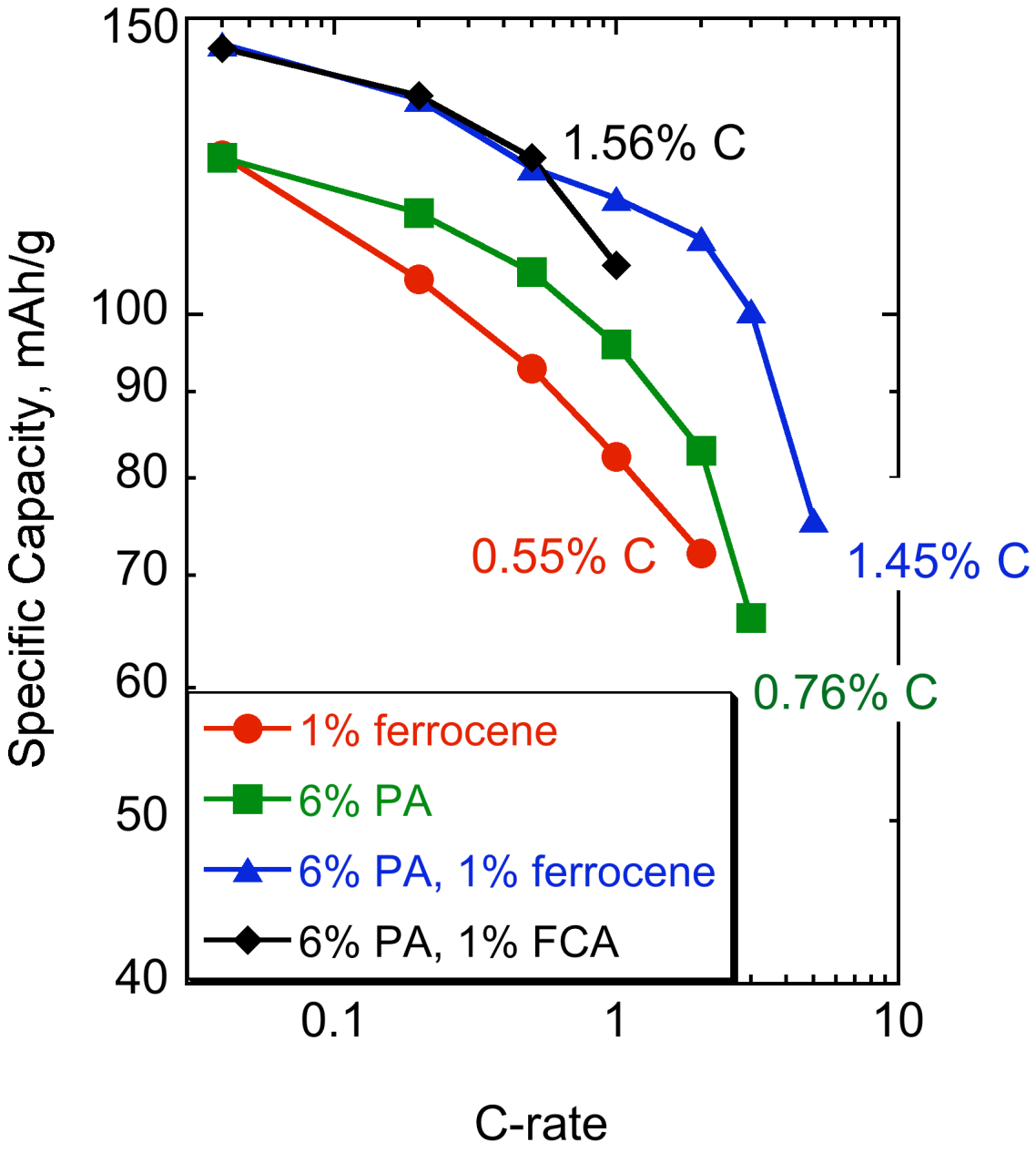
150
100
90
80
70
60
50
40
0.1
1
10
Specific Capacity, mAh/g
C-rate
1.56% C
0.55% C
1.45% C
0.76% C
1% ferrocene
6% PA
6% PA, 1% ferrocene
6% PA, 1% FCA

Figure 7

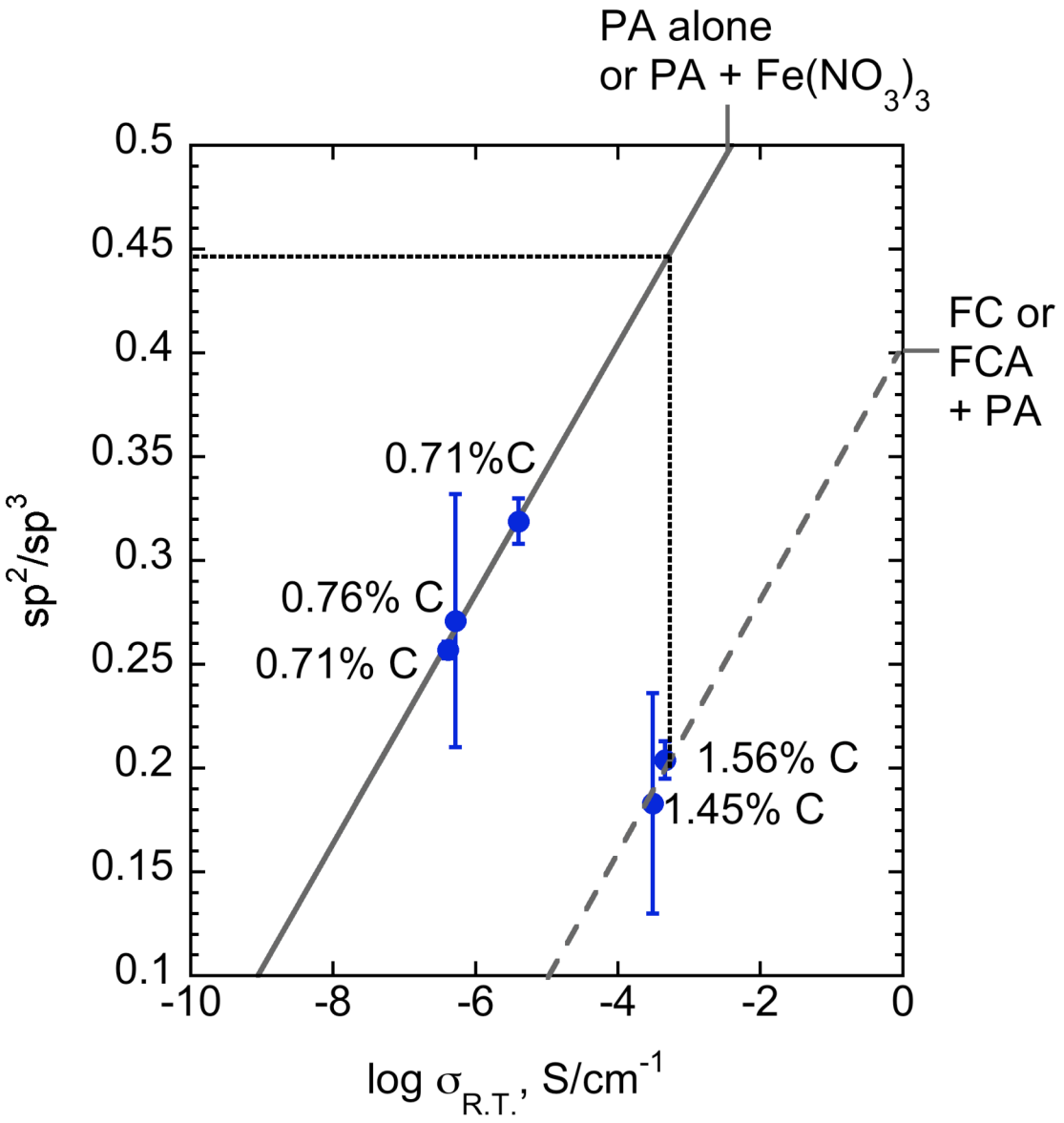
PA alone
or PA + Fe(NO3)3
FC or
FCA
+ PA
0.71%C
0.76% C
0.71% C
1.56% C
1.45% C
sp2/sp3
log σR.T., S/cm-1
0.5
0.45
0.4
0.35
0.3
0.25
0.2
0.15
0.1
-10
-8
-6
-4
-2
0

Figure 8

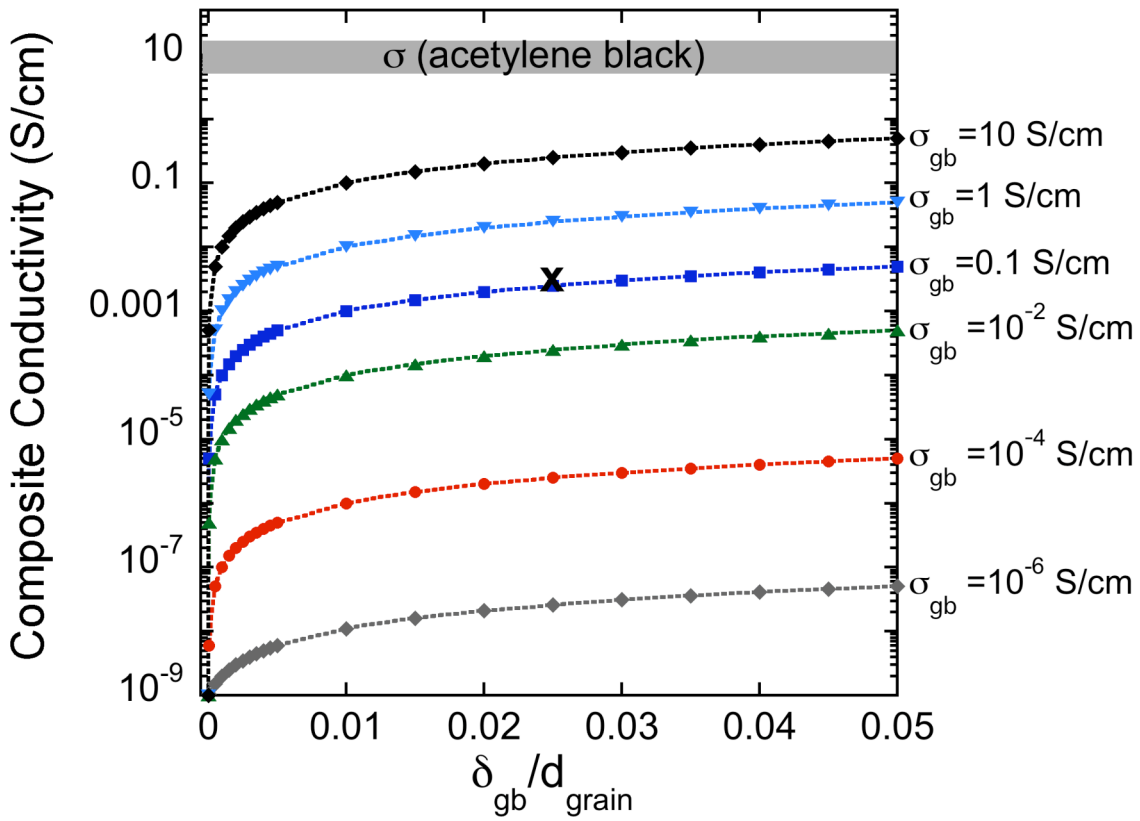
Composite Conductivity (S/cm)
10
0.1
0.001
10-5
10-7
10-9
σ (acetylene black)
σgb =10 S/cm
σgb =1 S/cm
σgb =0.1 S/cm
σgb =10-2 S/cm
σgb =10-4 S/cm
σgb =10-6 S/cm
0
0.01
0.02
0.03
0.04
0.05
δgb /dgrain

Figure 9